SLAC-PUB-10400
April 2004

Future Possibilities for the SPEAR3 Lattice

M. Cornacchia,† W. Corbett, R. Hettel, Y. Nosochkov,
T. Rabedeau, J. Safranek, A. Terebilo, and M. Yoon‡
Stanford Linear Accelerator Center

Abstract

This paper describes the modifications that can be made to the SPEAR3 baseline lattice in order to optimize the match of the electron optics for future insertion devices. The latter include an in-vacuum undulator and other devices specially tailored for hard x-ray sources. The common requirement of these sources is a small vertical electron beam size at the insertion devices that will allow the use of small gap undulators. Thus, the goal of this study is to show the feasibility of installing in SPEAR3 a lattice with β_y-functions at the insertion devices straight sections that are smaller than the one provided by the baseline lattice. This modification has repercussions on the hardware configuration, the dynamic aperture and the lifetime.

†cornacchia@slac.stanford.edu
‡On leave from Dept. of Physics, POSTECH, San 31, Hyoja-dong, Nam-gu, Pohang, Gyeongbuk, 790-784 Korea

Supported in part by the Department of Energy Contract DE-AC03-76SF00515

Stanford Linear Accelerator Center, Stanford University, Stanford, CA 94309

I. INTRODUCTION

This paper is articulated in the following way. The rationale for small gap undulators opens the discussion in Section II. The baseline lattice, successfully commissioned [1] and currently in operation, is reviewed in Section III. Section IV describes and discusses a lattice where the β_y-functions in the long straight sections and in the matching cell straight sections are reduced from ~ 5 m to 2 m. In Section V an attempt is made to derive the dependence of the maximum possible length of the insertion devices on the β_y-function, as the latter is further reduced towards very small values.

The long, 7.6 m, straight section makes it possible to consider installing a "double waist optics" at the center of two chicanes. This solution allows the use of two undulators in the long straight section with the light emitted in directions that allows sufficient separation between the beamlines. Such lattice appears to be feasible and is presented in Section VI.

II. THE RATIONALE FOR SMALL GAP UNDULATORS

Increasingly, atomic scale information underlies scientific and technological progress in disciplines ranging from pharmaceutical development to materials synthesis to environmental remediation. While a variety of research tools are used to provide atomic scale information, techniques utilizing synchrotron radiation are proving invaluable. There is a broad diversity of synchrotron-based measurement techniques and associated beam requirements; however, an important class of techniques demands high brightness sources that produce large photon fluxes per unit source phase space. It is this class of experiments that is best served by undulator insertion devices on third generation light sources. The three pioneering 6-8GeV third generation light sources feature undulators operating in the 5-25 keV range on the radiation fundamental and lowest harmonics where undulator brightness approaches theoretical predictions even if the magnetic field quality is less than ideal. As undulator technology has matured, magnetic pole field shimming has proved a viable means to correct undulator fields such that now nearly theoretical brightness is obtained at higher harmonics. This development, coupled with recent work on small gap undulators, demonstrate that undulator

sources on third generation, intermediate energy rings (2.5-4.0 GeV) can serve many of the demands of high brightness hard X-ray research.

With the completion of the SPEAR upgrade, SPEAR3 provides the low emittance and high operating current required for high brightness beams in the hard X-ray regime. As such, SPEAR3 opens new opportunities for high brightness, hard X-ray research at SSRL. To fully exploit this opportunity, SSRL must look to adding undulator sources specifically tailored to produce hard X-ray radiation.

There are two competing technologies for such insertion devices. Superconducting undulators offer the promise of superior performance well suited to the needs of high brightness research on intermediate energy light sources. Superconductor technology as applied to undulator magnets, however, is still immature. Many technical issues must be resolved before such technology can be considered for an operational source. The alternative technology utilizes small physical gaps between the undulator magnet arrays to produce the high field, short period magnetic structure required for high brightness, hard X-ray beams from a intermediate energy light source. This technology is considerably more mature with operational small gap sources at all three high energy third generation light sources as well as the prototype device at NSLS.

Since the magnetic field strength scales roughly as exp(-gap/period) and brightness scales roughly as the square of the number of magnetic periods, any reduction in the magnetic gap permits an associated reduction in the magnetic period length which for a given undulator overall length translates to improved source brightness. There are several strategies utilized to reduce the magnetic gap. Often the undulator magnetic structure is located inside the storage ring vacuum vessel thus eliminating the extra magnetic gap required for two walls of the vacuum vessel. In addition, at some light sources the vertical size of the charged particle beam is reduced through use of focusing magnets to permit use a smaller magnet gap while retaining a given storage ring beam lifetime.

The effect of reducing the magnetic gap on undulator brightness is best illustrated through an example. In Fig.1 the brightness of two undulators is depicted. Undulator U20 is a 2.0 m insertion device with a 20.0 mm magnetic period and 6.0 mm magnetic gap. It is

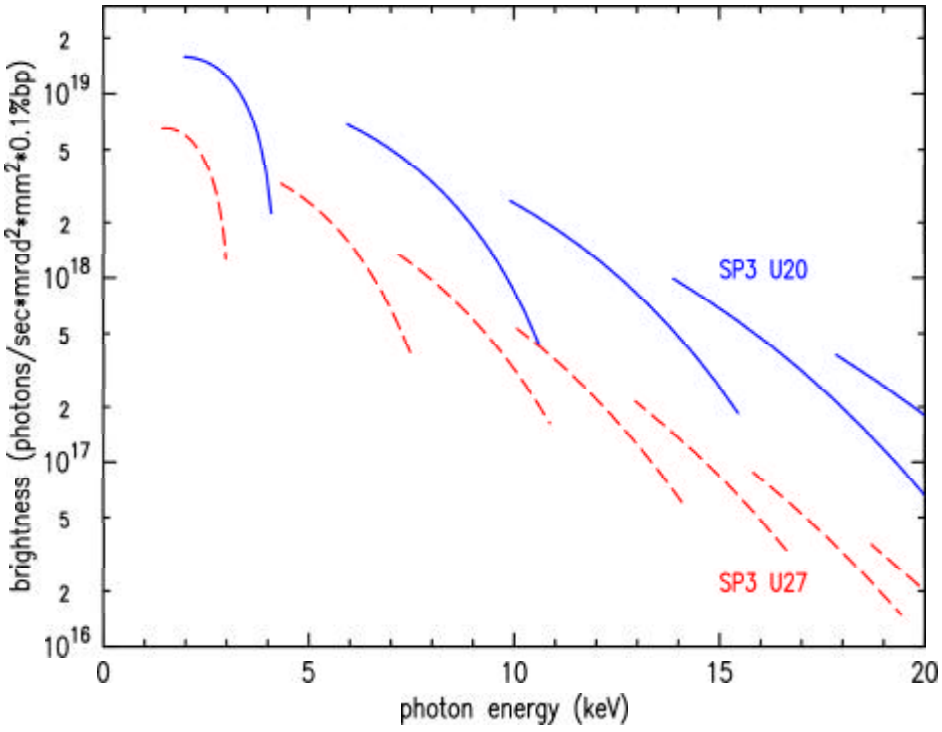

FIG. 1: Fundamental and odd harmonic tuning curves for two representative undulators with different β_{y0} and, correspondingly, different magnetic gaps scaled as Eq. 1 and shown in Fig.9

representative of an in-vacuum undulator located in the SPEAR3 East Pit drift straight, assuming a β_{y0} reduction from 5.5 m to 2.0 m, with β_{x0}= 8.0 m. The $\beta_{x,y}-$functions at the center of the straight section, and at the center of the undulator, are indicated as $\beta_{x0,y0}$. For comparison, the performance of U27,also a 2.0 m insertion device but with a 27.0 mm magnetic period and a 10 mm magnet gap is given for the baseline values of the electron optics (5.5 m β_{y0}, 8.0 m β_{x0}). The brightness plots assume a 18.6 nm-rad emittance and 0.1% energy spread. Magnetic undulator errors were not included in the computations. In the energy range of interest, specifically 7-15 keV, the U20 brightness exceeds that of U27 by 3-5 fold. Moreover, U27 tends to operate at a higher harmonic number for a given energy. This renders U27 more sensitive to undulator magnetic field errors than U20 at the same photon energy. Typical energies of interest range from 7 keV to 15 keV where U20 operates

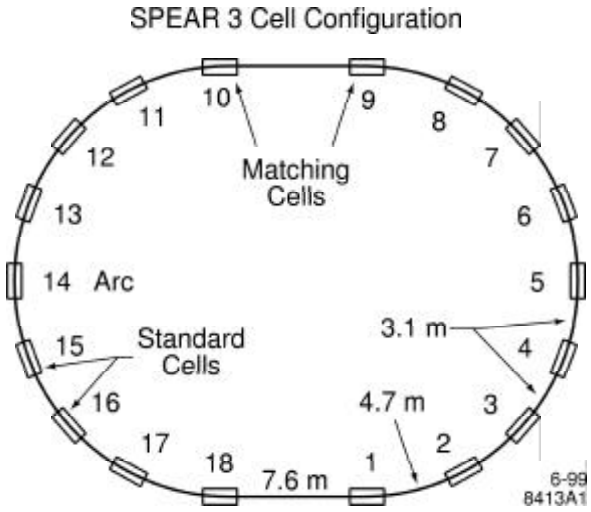

FIG. 2: Layout of SPEAR cells.

on the third through seventh harmonics. Over the same energy range U27 utilizes the fifth through the ninth harmonics.

III. THE BASELINE LATTICE

Fig.2 illustrates the cells in the SPEAR3 lattice. The circumference is 234.144 m. The lattice has two-fold symmetry . The total number of cells is 18, of which 14 are standard cells and four matching cells. Fig. 3 depicts the lattice functions. The parameter of main interest in this study are the following:

- Half-length of 14 standard cells straight: 1.53 m
- Half-length of 4 matching cells straight: 2.35 m
- Half-length of 2 long straights straight: 3.80 m
- β_{y0} in the standard and matching straight sections: 4.8 m.
- β_{y0} in the long straight sections: 10 m.

For the tunes of 14.19/5.23 (hor./vert.), the horizontal and vertical phase advances of the standard cell are $0.785\times2\pi$ and $0.259\times2\pi$ radians, respectively. In the matching cell, they are $2\times0.8\times2\pi$ and $2\times0.4\times2\pi$ radians, resulting in machine tunes of 14.19 and 5.23. In each matching cell there are two sets of sextupole families, SFI and SDI, with strengths, B"/Bϱ, of +15 and -17 m^{-3} respectively.

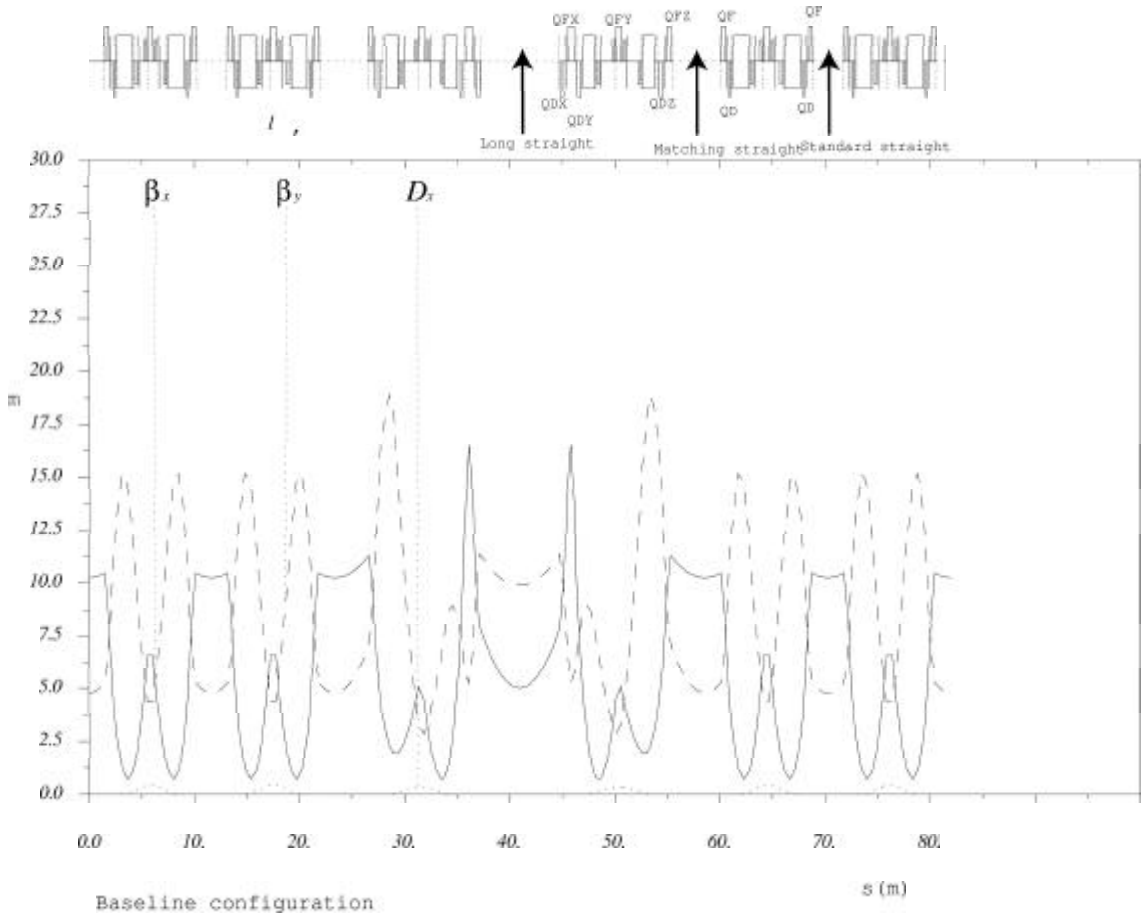

FIG. 3: Matching and adjacent standard cells in the baseline lattice.

A Dynamic aperture

Fig.4, plot A, depicts the dynamic aperture of the baseline lattice currently in operation. Plotted are the on-momentum particle and for those with $\triangle$P/P=$\mp$1%, $\mp$2%, $\mp$3%. The simulations of the three plots in Fig. 4 tracked the particles for 1000 turns and 30 "machines" with random error seeds having the following characteristics:

• No orbit errors were assumed.

• Quadrupole and skew quadrupole errors were introduced in the sextupoles only. Their strength was scaled to yield exactly 1%$\beta-$functions beats in horizontal and vertical planes. The random quadrupole misalignment was weighted to produce and 1% emittance coupling.

• Systematic and random multipole errors of orders sextupole and above were included.

In Fig. 4the bands correspond to the range of dynamic aperture for 30 machines.

IV. A MODIFIED SINGLE-WAIST LATTICE WITH β_{Y0}= 2 M

As Fig.3 shows, β_{y0} in the matching straight sections (adjacent straights on each side of the 7.6 m long straight sections) is 4.8 m. Of the four available matching straight sections, two in the east arc are reserved for two new insertion devices, and therefore it is advantageous to have smaller β_{y0} there. However, it is convenient, for reasons of dynamic aperture, to preserve the two-fold symmetry of the ring. For this reason, the east and west cells are kept the same. Fig.5 shows one such solution, *which has lower β_{y0} in the matching and in the long straights , 2.05 m and 2.0 m respectively* (as compared to the 4.8 and 10 meters of the baseline optics). The modified lattice described in this Section will be referred to as *modified single-waist* to distinguished it from the double waist described in Section VI. In this optics the phase advances in both the standard and matching cells have been re-arranged in order to keep the tunes the same as those of the baseline design, 14.19 and 5.23. Since the vertical phase advance of the standard cell is smaller than that of the baseline optics, β_{y0} in the standard straight sections increases from 4.8 m to 6.05 m. This causes a 3.6 μm (i.e. approximately 12 %) increase in beam size for 1% coupling and a 6 μm increase for 3% coupling. Table I compares some of the baseline lattice parameters with those of the new optics.

Table II shows the quadrupole and sextupole strengths of the new configuration as compared with those for nominal optics. The strengths of the QDe and QDw quadrupoles which are the horizontally defocussing quadrupoles in the standard cells adjacent to the east-pit and west-pit matching straights respectively, have been increased by approximately 44 % but their strength is still lower than the maximum strength that these magnets can provide (2.0 m^{-2}) at 3.3 GeV . The gradient of the other quadrupoles are well under their maximum strengths. The two-fold machine periodicity has thus been retained and the strengths of the QDe and QDw quadrupoles are the same. Table II reports the values of the quadrupoles and

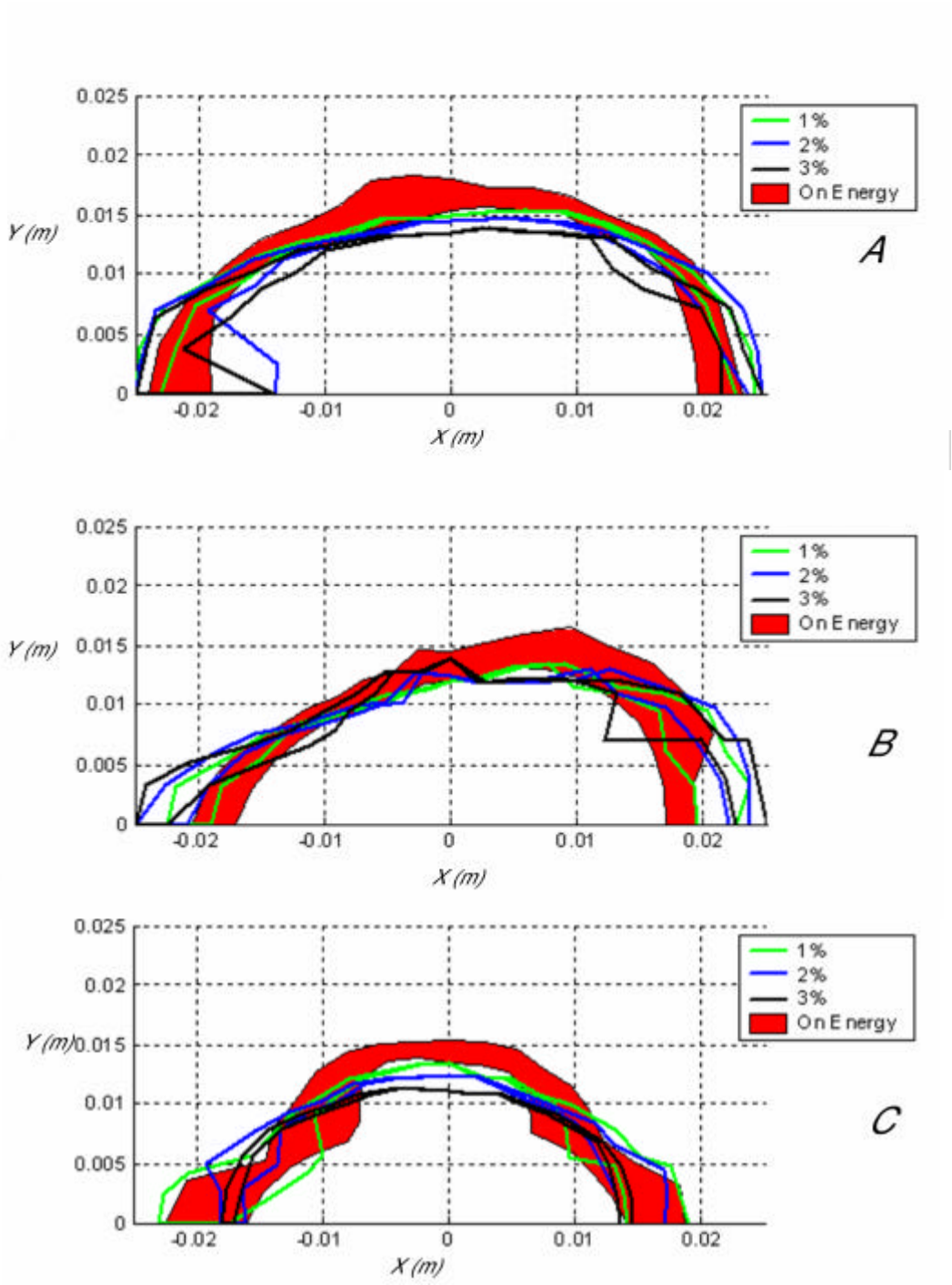

FIG. 4: Dynamic aperture of the baseline optics (A), of the modified single-waist optics (B), described in Section IV and of the low β_{y0} doublewaist optics (C), described in Section VI.

.

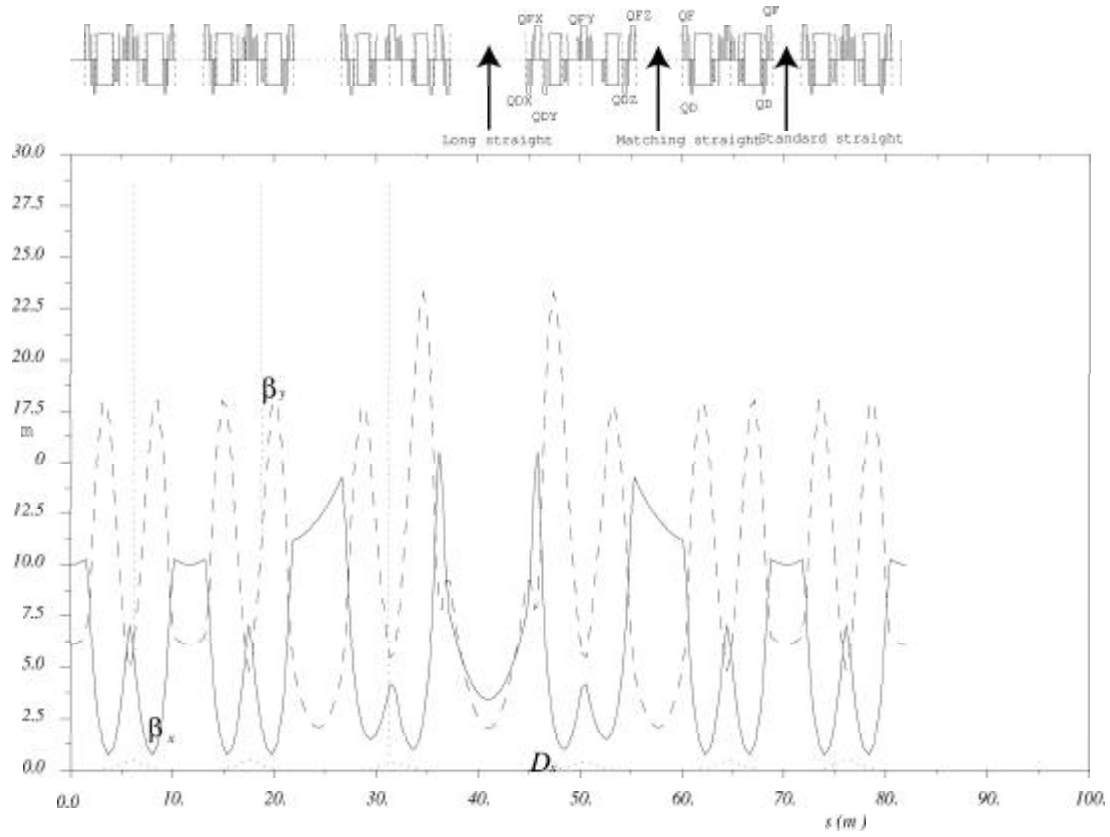

FIG. 5: Matching and adjacent standard cells in the lower β_{y0} configuration.

sextupoles for the baseline and the new optics. The dynamic aperture of the modified lattice presented in this Section is shown in Plot (B) of Fig. 4 with the simulation data described in III A. Its behaviour is not significantly different from that of the baseline lattice. In fact, the same low β_y optics in the long straight section (but not yet in the matching cells since this requires a different arrangement of power supplies) has been tested experimentally in SPEAR3 [2]: its lifetime and ease of operation was no different from that of the baseline lattice.

V. PARAMETRIC OVERVIEW AND TRADE-OFFS BETWEEN INSERTION DEVICE LENGTH AND β_{Y0}-FUNCTION IN THE SINGLE WAIST LATTICE

It has been shown that the lattice with the characteristics described in the previous Section is feasible. It reduces the vertical β_y-function in the IDs of the matching and long

TABLE I: Some parameters of the baseline and of the modified single-waist optics.

Parameters	Baseline optics	Low β_{y0} optics in matching and long straight sections
Tunes(hor/vert)	14.19	5.23
Natural emittance, nm-rad	18	18
Natural chromaticities (hot/vert)	-22.1/-14.3	-21.6/-17.4
Maximum β_{x0}, m	14.6	14.2
Maximum β_{y0}, m	18.2	21.9
β_{x0}/β_{y0}, m, in standard cell straight sections	10.2/4.8	10.0/6.1
β_{x0}/β_{y0}, m, in matching cell straight sections	10.2/4.8	11.7/2.0
β_{x0}/β_{y0}, m, in long straight sections	5.0/9.9	3.4/2.0

straights. It would be useful to explore how far one could go in lowering the β_y-functions and what the implications for the lengths of the insertion devices would be without compromising the performance of the storage ring. A complete self-consistent ring lattice calculations for a large number of combinations of these parameters would impose a heavy burden in terms of effort and computing time. It was chosen instead to tackle the problem using a simplified system that approximates the focussing magnets in the straight sections to thin focussing lenses. The analysis is applied independently to the matching and the long straight sections. Fig. 6 shows the magnetic layout of the long and matching cells with their straight sections.

Only the vertical plane is considered and the quadrupoles are approximated thin lenses.

A The matching straight section

The matching cell of Fig. 6 is contained within the two vertical lines that pass through the center of the straight sections and of the length of the so called, in the SPEAR3 nomenclature

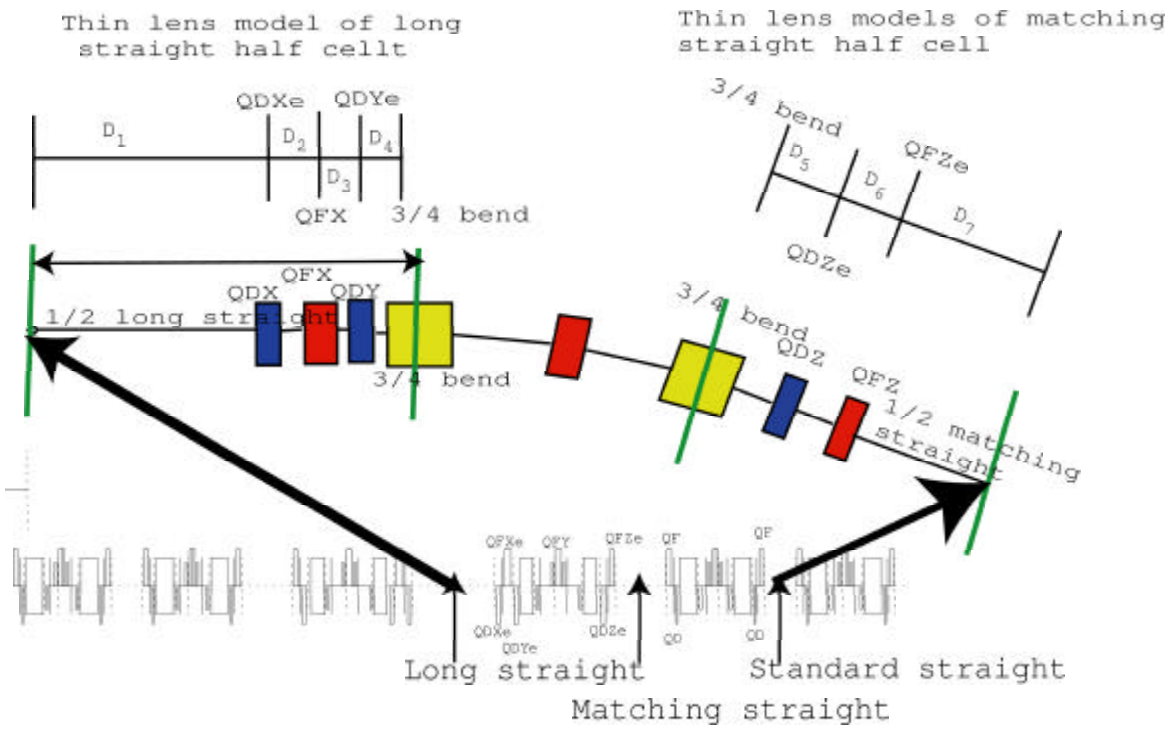

FIG. 6: The figure depicts the magnetic layout of the long straight sections, the matching straight sections and the standard straight sections . The first two are enlarged and the thin lens models used for the analysis are shown at the top of the page.

"3/4 length" bend (since its length is in this ratio to that of the standard bends). This magnet also has a gradient field that focusses the beam vertically. For the low β_{y0} lattice described in Section IV, the β_y function has a minimum at the half-length of the straight section and a maximum approximately at the half-length the 3/4 bend (see the lattice functions of Fig. 5). In this study the assumption is made that any reasonably well behaved lattice will preserve the waist and the maximum β_{y0} at the same location, even as the length of D_7 is varied.

Still referring to Fig. 6, the equations of the linear electron optics of the matching straight was solved with the following boundaries:

∘ The maximum half-length of the insertion device, $L_{\frac{1}{2}ID} = D_7 - D_{overhead}$, and the β_{y0} value at its center were varied within the region $0.1 \leq \beta_{y0} \leq 2.0$ m. $D_{overhead}$, 0.543 m, is the length that is occupied by the baggage of vacuum hardware and the half length of the magnet QFZe in Fig. 6.

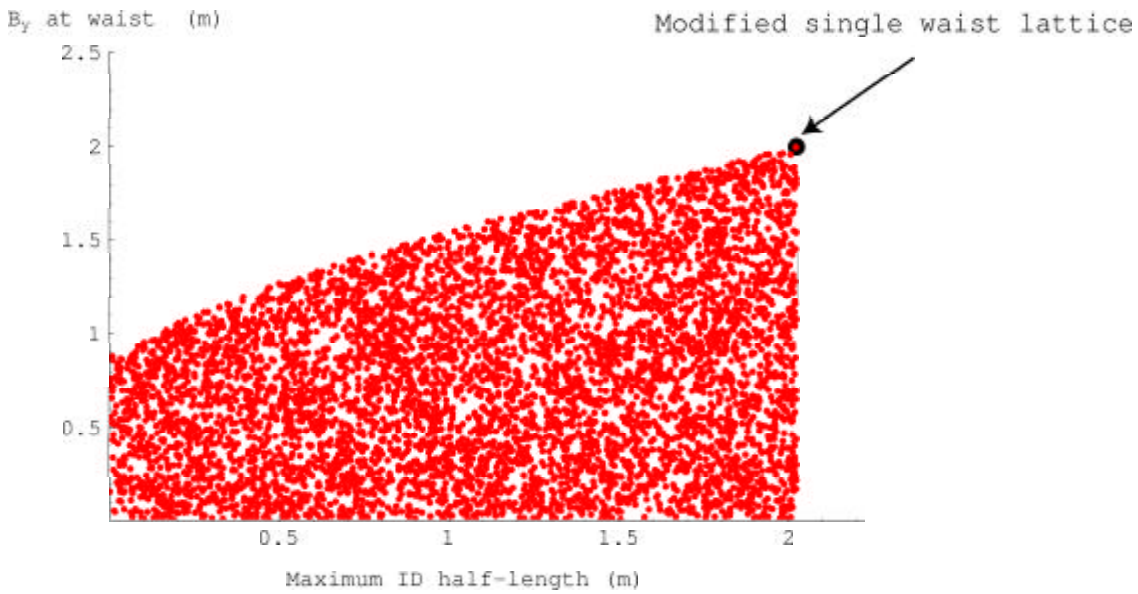

FIG. 7: The shadow part of the figure shows the region where the β_{y0} and the half length of the ID *in a matching cell* result in a chromaticity that is larger than the one of the modified single-waist lattice of Section IV. In the clear area the reverse is true. The latter should yield a dynamic aperture not smaller than the that of case B of Fig. 4

.

∘ The optics has a waist at about the middle of the ID: β'_{y0}=0

∘ The distance from the 3/4 bend to the half-length of the matching straight is fixed at the baseline value of D_{match}=4.541 m.

∘ D_5 varies as D_5=D_{match}-D_6-D_7, which is equivalent to moving the doublet QDZe, QFZe with respect to other magnets in order to change the ID length..

∘ The integrated gradient of the 3/4 bend and QFZe are kept fixed at their baseline values.

∘ The vertical optics equations are solved for β'_{y0}=0 in the middle of the 3/4 bend and for the strength of the QDZe lens.

The horizontal plane was not considered, i.e. no re-matching based on horizontal optics considerations was performed.

In spite of its extreme simplicity, this model should give some directions to the choice of low β_{y0} lattices and their ID lengths. The results of this model are depicted in Fig. 7. Apart from the details of the plot, Fig. 7 indicates that the β_{y0}-function can be reduced to < 1.2

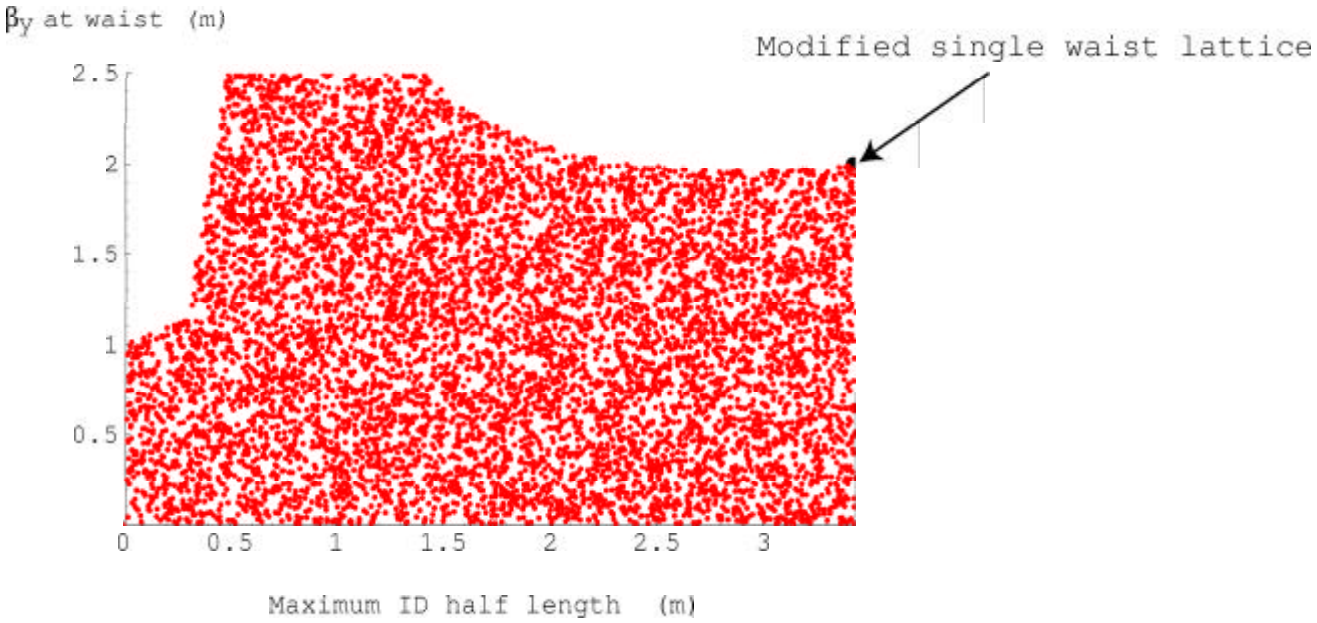

FIG. 8: The shadow part of the figure shows the region where the β_{y0} and the half length of the ID in the *long straight section* result in a chromaticity that is larger than the one of the modified single-waist lattice of Section IV. In the clear area the reverse is true. The latter should yield a dynamic aperture not smaller than the that of case B of Fig. 4

.

m without adverse effect for the dynamic aperture, provided that the ID half-length, and, correspondingly, the half-length of the straight section is reduced to below 0.5 m. *It should be clear that these results are critically dependent on the length occupied by the quadrupoles and other vacuum components (collectively called "overhead" in this report). Special, shorter and more compact design would allow for smaller β_{y0} with the same ID length, or, alternatively, longer ID lengths for the same β_{y0}.*

B The long straight section

A similar analysis for the long straight sections led to the allowed parametric region of Figure 8. The lattice parameters used in deriving the solutions of Figure 8 were the following: ∘ The maximum half-length of the insertion device, $\mathrm{L}_{\frac{1}{2}ID} = D_1 - D_{overhead}$, and the β_{y0} value at its center are scanned within the region $0.1 \leq \beta_{y0} \leq 2.0$ m.$\mathrm{D}_{overhead}$, 0.543 m, is the length

that is occupied by the baggage of vacuum hardware and the half length of the magnet QDXe in Figure 6. It is taken to be the same as that of the matching straight,

∘ The optics has a waist at the middle of the ID: $\beta_{y0}\prime$=0.

∘ The distance from the middle of the 3/4 bend to the center of the long straight section is fixed at the baseline value of D_{long} = D_1+D_2+D_3+D_4=4.541 m.

∘ D_2=0.56 m.

∘ D_3=0.44 m.

∘ D_4=D_{long}-D_1-D_2-D_3, which is equivalent to moving the triplet QDXe, QFXe, QDYe with respect to other magnets in order to change the ID length.

∘ The integrated gradient of the 3/4 bend, QDXE, QFXE and BND are kept fixed at their baseline values.

∘ The optics equations are solved requiring that β'_{y0}=0 in the middle of the 3/4 bend and for the strength of the QDYE lens. Fig. 8 indicates that, like with the matching cell straight, a β_{y0} smaller than 1.2 m is achievable, provided the half-length of the ID is less than 0.5 m. The system appears to be more sensitive to increased chromaticity for low β_{y0} than the simpler matching cell layout.

It should be re-emphasized what's already said in the previous section: *these results are critically dependent on the length occupied by the quadrupoles and other vacuum components (collectively called "overhead" in this report). Special, shorter and more compact design would allow for smaller β_{y0} with the same ID length, or, alternatively, longer ID lengths for the same β_{y0}.*

C Gap height of the insertions device

Assuming that the new insertion devices are designed to preserve the existing vertical acceptance, then the relationship between the physical vertical gap (2h), the ID length (2L) and β_{y0} is given by the expression

$$\frac{h^2}{\beta_{y0} \cdot (1 + \frac{L^2}{\beta_{y0}^2})} \geq vertical\ acceptance\ of\ baseline\ lattice = 6.7mm - mrad[3] \qquad (1)$$

and is shown graphically in Figure 9.

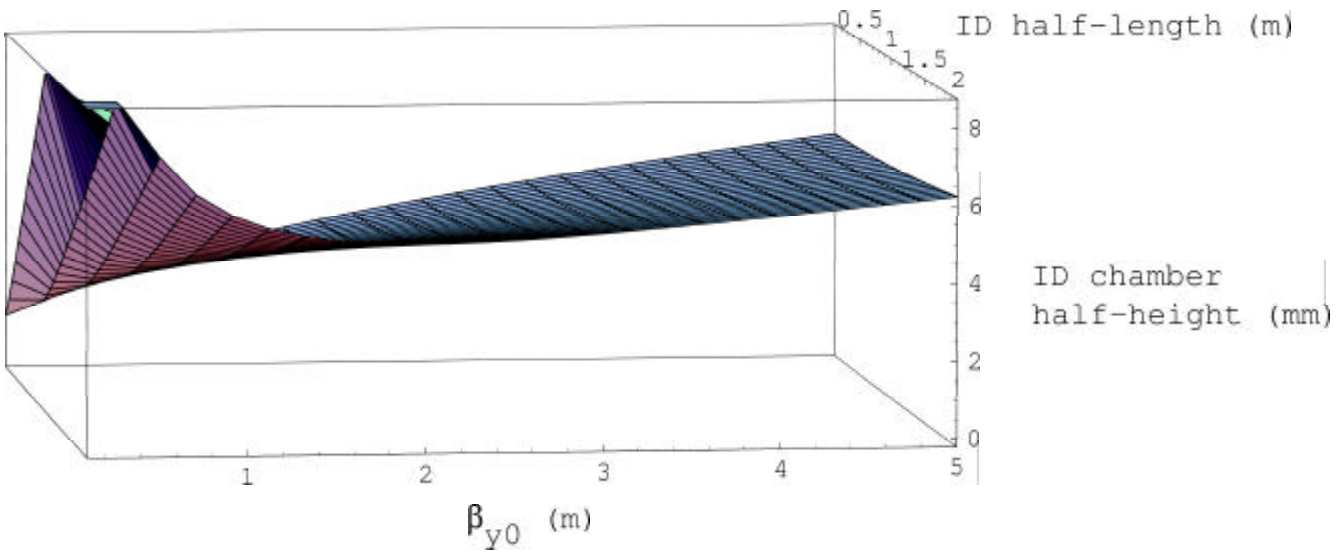

FIG. 9: Vertical minimum chamber half-height at the ID as a function of β_{y0} and the half-length of the ID for a vertical acceptance that is the same as that of the baseline design.

VI. THE DOUBLE WAIST OPTICS

The baseline SPEAR-3 lattice has identical symmetric optics in the east and west matching sections with a single beta waist at center of the 7.6 m straight section. The west straight section contains the accelerating RF-cavities, while the corresponding east space is available for insertion devices. One of the requirements for a small gap ID is a low vertical beta function. In Section II it was shown that it is desirable to reduce the vertical beta function at the ID location to 2 m or less. Another potentially attractive option is represented by having two IDs in the single east 7.6 m straight section. This optics requires two β_y waists on the same 7.6 m long straight section. A lattice modification of the east matching section to create symmetric double waist optics in the 7.6 m drift while at the same time reducing the vertical beta function at center of the two 4.8 m drifts is described below.

To create a double waist optics, a quadrupole triplet is added in the center of the long straight to focus the beam at two separate points. Symmetry with respect to the center of the straight was preserved by using a symmetric triplet QFE-QDE-QFE. Using standard type SPEAR3 quadrupoles in the triplet with 0.34 m and 0.6 m length results in about 1.8 m of usable free space on either side of the triplet where the IDs may be placed. The

positions of the low β_{y0} were chosen to be at center of these straights. In addition to the triplet quadrupoles, dipole magnets are needed to separate the photon flux generated in the two IDs. Four 0.25 m long bends are included, symmetrically in the two straights, to make a four-bend horizontal chicane. Using 5 mrad bends, the chicane creates 10 mrad angle between the two IDs which is sufficient for the separation of the photon beams.

Due to space limitation near the outside wall in the east tunnel hall, the chicane bends are designed to *direct the beam to the inside of the ring* with a maximum horizontal displacement of 11.85 mm. The chicane increases the beam path length by 57 μm compared to the baseline design. In this scheme, the free space between the bends is 1.8 m on each side of the triplet and where insertion devices may be installed.

Under this scheme, the east matching section will have 8 independent families of quadrupoles which are sufficient to create a matched symmetric optics with identical low beta points at the center of 2.1 m drifts for two IDs. The chicane bends generate a small, < 1 cm, dispersion in the 2.1 m straights, but this will be canceled outside of the east matching section. Quadrupole power supplies in the west section would have to be separate from the east quadrupoles in this lattice. Figure 10 shows the space available ($1.8m$) for each ID once realistic magnets and vacuum components are taken into account.

In addition to the double waist in the long straight sections, a successful attempt was made to lower the vertical beta function in the two 4.8 m drifts adjacent to the east matching section. Based on the lattice constraints and dynamic aperture, the vertical beta function was reduced to 1.6 m at the double waist positions in the east section and to 2.5 m in the two adjacent 4.8 m drifts. Table III shows the lattice parameters for this option, and Table IV lists the modified magnet strengths. Magnet names with the last letter "e" in Table IV correspond to the east matching section. The lattice functions in the east matching section are shown in Fig. 11. The dynamic aperture is the lowest plot C in Figure 4. This lattice requires 3 additional quadrupoles and 4 chicane bends in the east matching section, 4 quadrupole power supplies for the two arc cells and separate quadrupole power supplies in the east and west matching sections. A new section of vacuum chamber is also required for the south east matching cell to allow the separate photon beams to exit. Tables III, IV, V

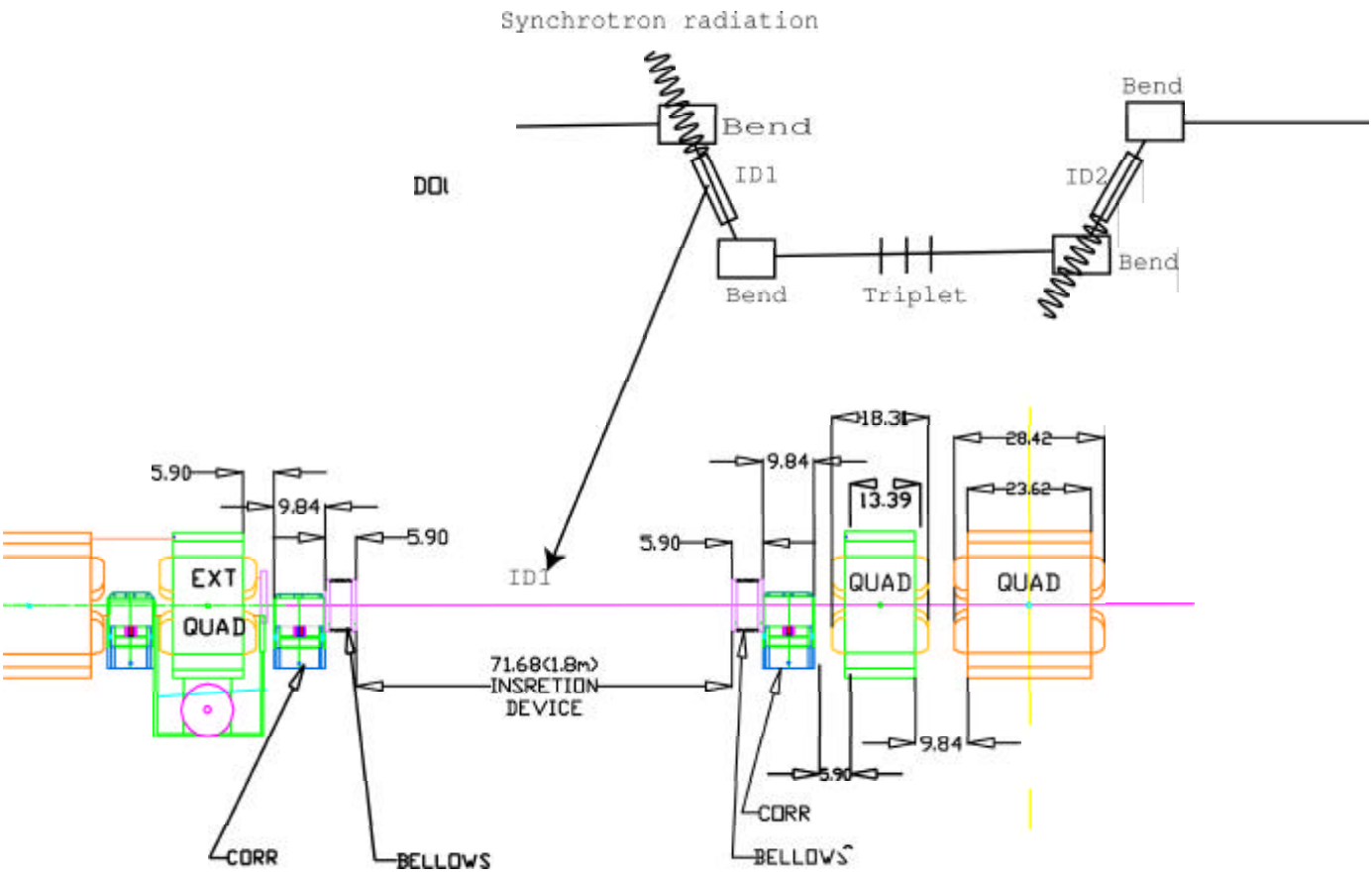

FIG. 10: This drawings shows the geometry of the IDs, the positions and the spaces occupied by the hardware of a double waist optics in the long straight section.

and VI provide the main lattice parameters and the quadrupole strengths.

VII. SUMMARY

The SPEAR3 lattice offers flexibility and potential for meeting the requirements of future insertion devices. Small gap undulators offer considerable enhanced performance, and require electron optics with lower β_y-function at the straight section hosting the insertion device. This implies the need for stronger focussing without compromising the dynamic aperture. The present baseline lattice has been successfully commissioned and a version of

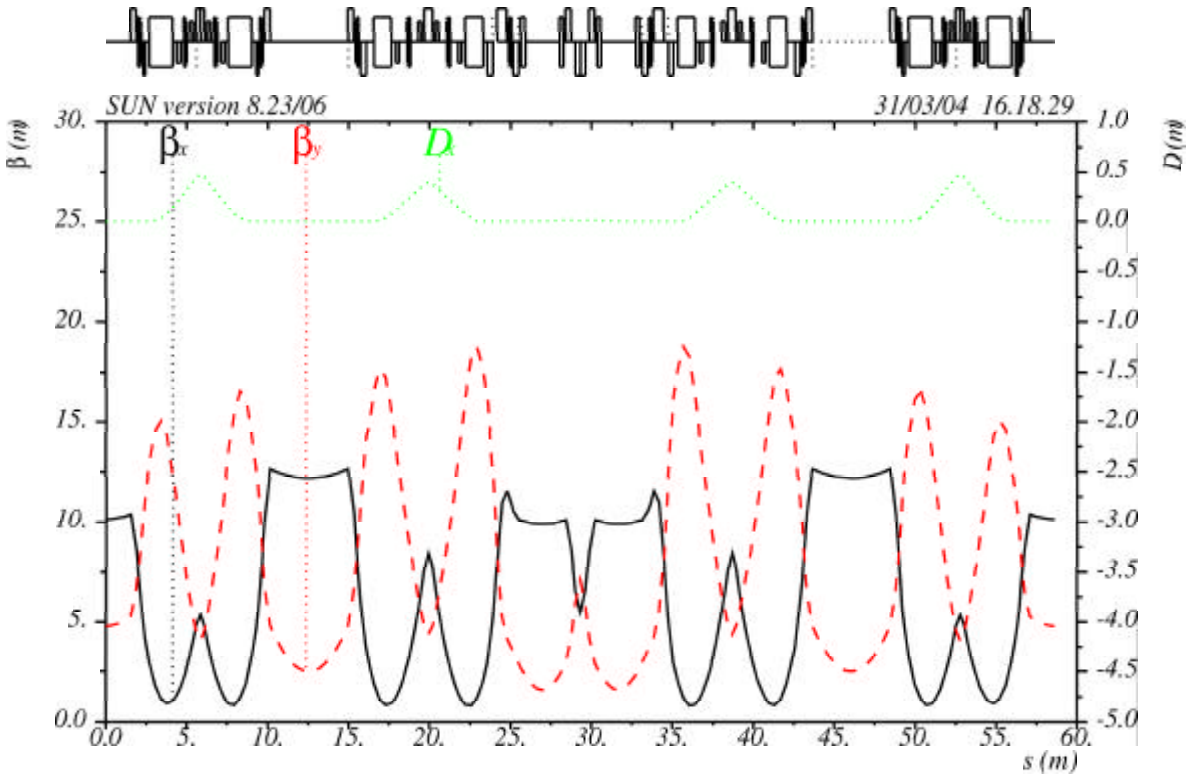

FIG. 11: Lattice function of the double waist optics in the long straight sections and reduced β_0 in the long and matching straight sections

it with a lower β_y also gave excellent operational performance. This study predicts that a further reduction in the single-waist low β_y-function optics is obtainable without major modifications to the hardware of the storage ring.

With modifications to the magnet consiguration a more aggressive double-waist optics can be achieved which allows two IDs in the 7.6 m east straight section.

The trade-offs between ID length and β_y-function have been analyzed using a simplified model for the electron optics.

This research was carried out at the Stanford Linear Accelerator Center, a national user facility operated by Stanford University on behalf of the U.S. Department of Energy, and was supported by the DOE Office of Science.

REFERENCES

[1] J. Safranek et al., "SPEAR3 Commissioning", Proceedings of the 2004 Asian Accelerator Conference.

[2] SPEAR3 Commissioning Results, unpublished.

[3] As given by the chamber half-height of 5.75 mm at β_y= 4.9 m.

TABLE II: Quadrupole and sextupole strengths for the baseline and low β_{y0} optics in matching and long straight sections.

Magnet	Baseline strengths	Low β_{y0} strengths	Units
QF	+1.7686729	+1.7147201	m^{-2}
QD	-1.5424742	-1.32921134	m^{-2}
QFC	+1.7486408	+1.7486408	m^{-2}
QFe	+1.7686729	+1.7525434	m^{-2}
QDe	-1.5424742	**-1.9092151**	m^{-2}
QFw	+1.7686729	+1.7525434	m^{-2}
QDw	-1.5424742	**-1.9092151**	m^{-2}
QFXe	+1.5731963	+1.71084301	m^{-2}
QDXe	-1.3864672	-1.17560098	m^{-2}
QFYe	+1.4814937	+1.48149228	m^{-2}
QDYe	-0.4606409	-1.14366995	m^{-2}
QFZe	+1.4279020	+1.5300754	m^{-2}
QDZe	-0.8782239	-0.90820157	m^{-2}
QFXw	Same as East-pit quadrupoles		
QDXw	Same as East-pit quadrupoles		
QFYw	Same as East-pit quadrupoles		
QDYw	Same as East-pit quadrupoles		
QFZw	Same as East-pit quadrupoles		
QDZw	Same as East-pit quadrupoles		
SF	+32.05	+32.82	m^{-3}
SD	-38.80	-39.78	m^{-3}
SFI	+15.0	+19.84	m^{-3}
SDI	-17.0	-26.21	m^{-3}

TABLE III: Lattice parameters in double waist option.

Circumference	234.144070 m
Betatron tune, x/y	14.19/6.23
Betas at double waist, x/y	9.9 / 1.6 m
Beta in 4.8 m East straight section, x/y	12.2 / 2.5 m
Beta in 4.8 m West drifts, x/y	10.1 / 4.8 m
Beta in 3.1 m drifts, x/y	10.1 / 4.8 m
Phase advance per cell, x/y	0.785 / 0.256429 [2pi]
Natural chromaticity, x/y	-22.6 / -15.4
Momentum compaction	1.14e-3
Horizontal emittance	18 nm rad
Synchrotron tune	8.3e-3
rms energy spread	1.0e-3
rms bunch length	5 mm

TABLE IV: Quadrupole strengths in double waist lattice.

Magnet	L (m)	K_1 (m^{-2})	K_1*L (m^{-1})
QF	0.34	1.813153	0.616472
QD	0.15	-1.566711	-0.235007
QDXw	0.34	-1.623454	-0.551974
QFXw	0.60	1.883360	1.130016
QDYw	0.34	-1.457632	-0.495595
QDZw	0.34	-1.227198	-0.417247
QFZw	0.34	1.673295	0.568920
QDXe	0.34	-0.283514	-0.096395
QFXe	0.60	1.285299	0.771179
QDYe	0.34	-1.312766	-0.446340
QFYe	0.50	1.516624	0.758312
QDZe	0.34	-0.990944	-0.336921
QFZe	0.34	1.697752	0.577236
QFe	0.34	1.457877	0.495678
QDe	0.60	-1.990760	-1.194456
QFM1	0.34	1.815178	0.617161
QDM1	0.15	-1.999967	-0.299995
QFM2	0.34	1.674152	0.569212
QDM2	0.15	-1.361331	-0.204200

TABLE V: Sextupoles strengths in double waist lattice for chromaticities = +1.

Magnet	L (m)	K2 (m^{-3})	K2*L (m^{-2})
SD	0.25	-39.982628	-9.995657
SF	0.21	32.785150	6.884882
SDI	0.21	-19.860068	-4.170614
SFI	0.21	15.132899	3.177909

TABLE VI: Chicane bends in double waist option.

Name	Number	L (m)	Angle (rad)
BEP	2	0.25	0.005
BEM	2	0.25	-0.005